Yrast structure of neutron-rich ^{53}Ti

B. Fornal,[1] S. Zhu,[2] R. V. F. Janssens,[2] M. Honma,[3] R. Broda,[1] B. A. Brown,[4,5] M. P. Carpenter,[2] S. J. Freeman,[2,6] N. Hammond,[2] F. G. Kondev,[7] W. Królas,[1,8] T. Lauritsen,[2] S. N. Liddick,[4,9] C. J. Lister,[2] S. Lunardi,[10] P. F. Mantica,[4,9] N. Marginean,[11] T. Mizusaki,[12] E. F. Moore,[2] T. Otsuka,[13,14] T. Pawłat,[1] D. Seweryniak,[2] B. E. Tomlin,[4,9] C. A. Ur,[10] I. Wiedenhöver,[2] and J. Wrzesiński[1]

[1]*Institute of Nuclear Physics, Polish Academy of Sciences, PL-31342 Cracow, Poland*
[2]*Physics Division, Argonne National Laboratory, Argonne, Illinois 60439, USA*
[3]*Center for Mathematical Sciences, University of Aizu, Tsuruga, Ikki-machi, Aizu-Wakamatsu, Fukushima 965-8580, Japan*
[4]*National Superconducting Cyclotron Laboratory, Michigan State University, East Lansing, Michigan 48824, USA*
[5]*Department of Physics and Astronomy, Michigan State University, East Lansing, Michigan 48824, USA*
[6]*Schuster Laboratory, University of Manchester, Manchester M13 9PL, United Kingdom*
[7]*Nuclear Engineering Division, Argonne National Laboratory, Argonne, Illinois 60439, USA*
[8]*Joint Institute for Heavy Ion Research, Oak Ridge, Tennessee 37831, USA*
[9]*Department of Chemistry, Michigan State University, East Lansing, Michigan 48824, USA*
[10]*Dipartimento di Fisica dell'Università di Padova, and INFN Sezione di Padova, I-35131 Padova, Italy*
[11]*INFN, Laboratori Nazionali di Legnaro, I-35020 Legnaro, Italy*
[12]*Institute of Natural Sciences, Senshu University, Higashimita, Tama, Kawasaki, Kanagawa 214-8580, Japan*
[13]*Department of Physics, University of Tokyo, Hongo, Tokyo 113-0033, Japan*
[14]*RIKEN, Hirosawa, Wako-shi, Saitama 351-0198, Japan*

(Received 22 June 2005; published 27 October 2005)

γ rays from neutron-rich Ti nuclei in the vicinity of $N = 32$ have been studied at Gammasphere using deep-inelastic reactions induced by ^{48}Ca beams on thick ^{208}Pb and ^{238}U targets. The ^{53}Ti yrast cascade was identified for the first time, and the location in energy of states with spin up to $I = 21/2$ was determined. The excitations of ^{53}Ti provide new tests of effective interactions for full-*pf*-shell calculations. Comparisons between theory and experiment for the highest spin states in ^{53}Ti favor the recently proposed GXPF1A interaction, which accounts for the appearance of a neutron subshell closure at $N = 32$ in Ti isotopes as well as for the lack of a similar subshell closure at $N = 34$, as predicted by earlier calculations with another interaction.

DOI: 10.1103/PhysRevC.72.044315 PACS number(s): 21.60.Cs, 23.20.Lv, 27.40.+z, 25.70.Lm

I. INTRODUCTION

Unforeseen modifications to the shell structure of neutron-rich nuclei have been observed recently, and it is possible that traditional magic numbers are no longer valid away from the valley of stability. One of the possible causes for the reordering of single-particle orbits, and for the resulting development of new subshell closures, is the proton-neutron monopole interaction [1]. Examples of such structural changes include the appearance of an energy gap at $N = 32$ for neutron-rich nuclei just above ^{48}Ca. This phenomenon, first suggested by Huck *et al*. [2], was recently confirmed in studies of 2^+ excitations in ^{56}Cr$_{32}$ and ^{58}Cr$_{34}$ [3] and in studies of the yrast structures in ^{54}Ti$_{32}$ [4] and ^{56}Ti$_{34}$ [5–7]. Nothing was known, however, about excited states in the odd titanium isotopes close to $N = 32$. These excitations, involving an odd neutron in either the $p_{3/2}$, $p_{1/2}$, or $f_{5/2}$ single-particle states, may serve as a sensitive probe of the location in excitation energy of these orbitals.

The yrast states of ^{54}Ti and ^{56}Ti were studied in Refs. [4,7] with deep-inelastic reactions occurring during the collisions of a ^{48}Ca beam with ^{208}Pb and ^{238}U targets at energies ~20% above the Coulomb barrier. Production of neutron-rich species in such processes is possible because of a tendency toward N/Z equilibration of the dinuclear system formed during the collision [8–10]. In the reactions under investigation, the light colliding partner ^{48}Ca had a lower N/Z ratio than the target, and as a result, production of nuclei with larger neutron excess than ^{48}Ca was favored. In the case of the titanium products, yields sufficient for γ-γ spectroscopic studies extended in neutron number up to ^{54}Ti for the ^{48}Ca+^{208}Pb system and up to ^{56}Ti for the ^{48}Ca+^{238}U reaction. The exploration of the yrast level structure of ^{54}Ti and ^{56}Ti was made possible by combining γ-ray spectroscopy following deep-inelastic reactions with β-decay measurements of ^{54}Sc and ^{56}Sc fragmentation products. The lowest γ ray (i.e., the $2^+ \rightarrow 0^+$ transition) in ^{54}Ti and ^{56}Ti could be unambiguously identified in β-decay studies, and subsequently used as the starting point in the analysis of the γ-γ coincidence data from deep-inelastic reactions [4,6,7]. In such a way, the higher-spin yrast structures were traced up to $I^\pi \sim 10^+$ in ^{54}Ti and up to $I^\pi \sim 6^+$ in ^{56}Ti.

From the observed production yields of the $^{48-52}$Ti, ^{54}Ti, and ^{56}Ti isotopes, it was clear that in both reactions the odd-mass titanium isotope ^{53}Ti had to have been populated as well with cross sections sufficient for γ-γ spectroscopic studies. Identification, however, was a problem because no information on excited states in this nucleus was available prior to the present work. Here, low-lying γ-ray transitions of ^{53}Ti were unambiguously assigned by using peculiar characteristics of γ-ray spectroscopic studies with deep-inelastic reactions, e.g., by examining the cross-coincidence relationships between complementary Ti and Hg reaction products in the ^{48}Ca+^{208}Pb

reaction. These low-lying ^{53}Ti transitions served then as a starting point for the investigation of the higher yrast excitations in this nucleus.

II. EXPERIMENTAL PROCEDURE AND ANALYSIS RESULTS

The two experiments were performed at Argonne National Laboratory employing a ^{48}Ca beam from the Argonne Tandem Linear Accelerator System (ATLAS) and Gammasphere [11], which consisted of 101 Compton-suppressed Ge detectors. During the first run, a 305 MeV beam was focused on a 50 mg/cm^2 ^{208}Pb target. In the second, the projectile energy was 330 MeV and a 50 mg/cm^2 ^{238}U target was used. γ-ray coincidence data were collected with a trigger requiring three or more Compton-suppressed γ rays to be in prompt coincidence. Energy and timing information for all Ge detectors that fired within 800 ns of the triggering signal was stored. The beam, coming in bursts with $\sim$0.3 ns time width, was pulsed with $\sim$400 ns repetition time, providing clean separation between prompt and isomeric events. A total of 8.1×10^8 and 2.3×10^9 three- and higher-fold events were recorded in the first and second measurements, respectively. Conditions set on the $\gamma\gamma$ time parameter were used to obtain various versions of prompt and delayed $\gamma\gamma$ and $\gamma\gamma\gamma$ coincidence matrices and cubes covering γ-ray energy ranges up to $\sim$4 MeV.

In spectroscopic studies of deep-inelastic reaction products, the assignment of an unknown sequence of γ rays to a specific product may be possible by using the cross-coincidence relationships with transitions in reaction partners. In the present work with the ^{208}Pb target, complementary products in binary reactions leading to Ti isotopes are Hg nuclei, but a given Ti nucleus is in coincidence with several Hg partners because of neutron evaporation from the fragments after the collision. The situation is illustrated in Fig. 1(a), which presents the spectrum arising from a sum of double coincidence gates placed on known transitions in ^{196}Hg. This spectrum displays, as expected, known lines from ^{50}Ti, ^{51}Ti, ^{52}Ti, and ^{54}Ti. These are partners of ^{196}Hg associated with 10, 9, 8, and 6 evaporated neutrons, respectively. Further inspection of the spectrum revealed also the presence of unknown γ rays with energies of 1237 and 1576 keV. These two lines were also observed in spectra gated on transitions from the Hg isotopes with $A = 197$–200, which confirmed that they originate from a titanium product. It seemed plausible that the new transitions might belong to ^{53}Ti.

To pursue this hypothesis further, the identification method based on the intensity of γ rays in cross coincidence was applied. For the ^{50,51,52,54}Ti reaction products, the mean mass $A_{\rm av}$(Hg) of the complementary mercury fragments was determined from the Hg γ-ray intensities measured in coincidence with γ transitions belonging to the specific Ti isotope (see Ref. [8] for further details). The same procedure of calculating the Hg mean mass was also applied to the newly found 1237 and 1576 keV Ti lines. The results are illustrated in Fig. 2, where the $A_{\rm av}$(Hg) values are given as a function of the A(Ti) masses. The data points corresponding to the known γ rays in ^{50,51,52,54}Ti exhibit a smooth correlation. The $A_{\rm av}$(Hg) values for the two new transitions fit nicely into this pattern, if one assigns the 1237 and 1576 keV lines to ^{53}Ti. Thus, the correlation between $A_{\rm av}$(Hg) and A(Ti) of Fig. 2 provides strong evidence for the assignment of the 1237 and 1576 keV γ rays to the ^{53}Ti nucleus, and these two transitions then form the stepping stone for the construction of a more elaborate level scheme.

Based on the ^{48}Ca+^{208}Pb reaction data, a coincidence spectrum gated with the 1576 keV transition [Fig. 1(b)] shows four strong, mutually coincident γ rays with respective energies of 258, 292, 387, and 630 keV. The same sequence of γ rays is also present in a spectrum arising from the 1237 keV gate, but with an additional prominent transition of 339 keV (not shown). The coincidence relationships between the newly identified γ rays lead to the conclusion that (a) the 339–1237 keV cascade occurs in parallel with the 1576 keV transition and deexcites a level at 1576 keV (both the 1576 and 1237 keV γ rays are then ground-state transitions), (b) the sequence of transitions 630, 292, 258, and 387, with the crossover γ rays of 969 keV (339+630) and 922 keV (630+292), establish above the 1576 keV excitation the levels at 2206, 2498, 2756, and 3143 keV. The inspection of double coincidence gates placed on the lines identified so far [an example of which is shown in Fig. 1(c)] revealed the presence of additional weaker γ rays at 902, 1254, 1659, and 2586 keV. The observed coincidences and the measured intensities led to the level scheme proposed in Fig. 4 with additional states located at 4802, 5729, 6056, and 6630 keV. Further development of the ^{53}Ti yrast level structure was possible with the second $\gamma\gamma$ coincidence data set, obtained with the ^{48}Ca+^{238}U reaction. Representative $\gamma\gamma$ coincidence spectra from this reaction are displayed in Fig. 3. This data set was found to include $\sim$2.5 times more $\gamma\gamma$ events from ^{53}Ti than that from the ^{48}Ca+^{208}Pb reaction. The analysis of the ^{48}Ca+^{238}U data fully confirmed the level structure of ^{53}Ti deduced from the ^{48}Ca+^{208}Pb reaction and, in addition, identified a few weaker lines. Two of them, a 574 keV line [Fig. 3(b)] and a very weak 1828 keV transition, were found to deexcite the 6630 keV level toward the 6056 and 4802 keV states, respectively. In these higher statistics data, another new γ ray of 1501 keV energy appeared in coincidence with cascades deexciting the 6630 keV level [Figs. 3(b) and 3(c)] and was placed at the top of the level scheme of Fig. 4.

The high statistics acquired in the ^{48}Ca+^{238}U experiment made possible an analysis of the $\gamma\gamma$ angular correlations for selected pairs of transitions. Each detector in Gammasphere is associated with a pair of angles (ϑ, φ) with respect to the beam direction, and the angle between any two detectors can be obtained as $\cos(\delta) = \cos(\varphi_2 - \varphi_1) \times \sin(\vartheta_1)\sin(\vartheta_2) + \cos(\vartheta_1)\cos(\vartheta_2)$. In this analysis, all pairs of γ rays $(E_{\gamma_1}, E_{\gamma_2})$ with angles $20^\circ \leqslant \delta \leqslant 37^\circ$ were placed in one coincidence matrix, while those pairs with $83^\circ \leqslant \delta \leqslant 90^\circ$ were placed into another. In this way, about 1000 combinations of detectors are included in each matrix and about 2/5 of the total statistics is contained in just two matrices. The ratio between the intensities from each matrix at point $(E_{\gamma_1}, E_{\gamma_2})$ reflects the angular correlation between transitions γ_1 and γ_2 at angles 28° and 85° (on average). For a cascade of two stretched $E2$ transitions such as $4 \rightarrow 2 \rightarrow 0$, the ratio $I_\gamma(28^\circ)/I_\gamma(85^\circ)$

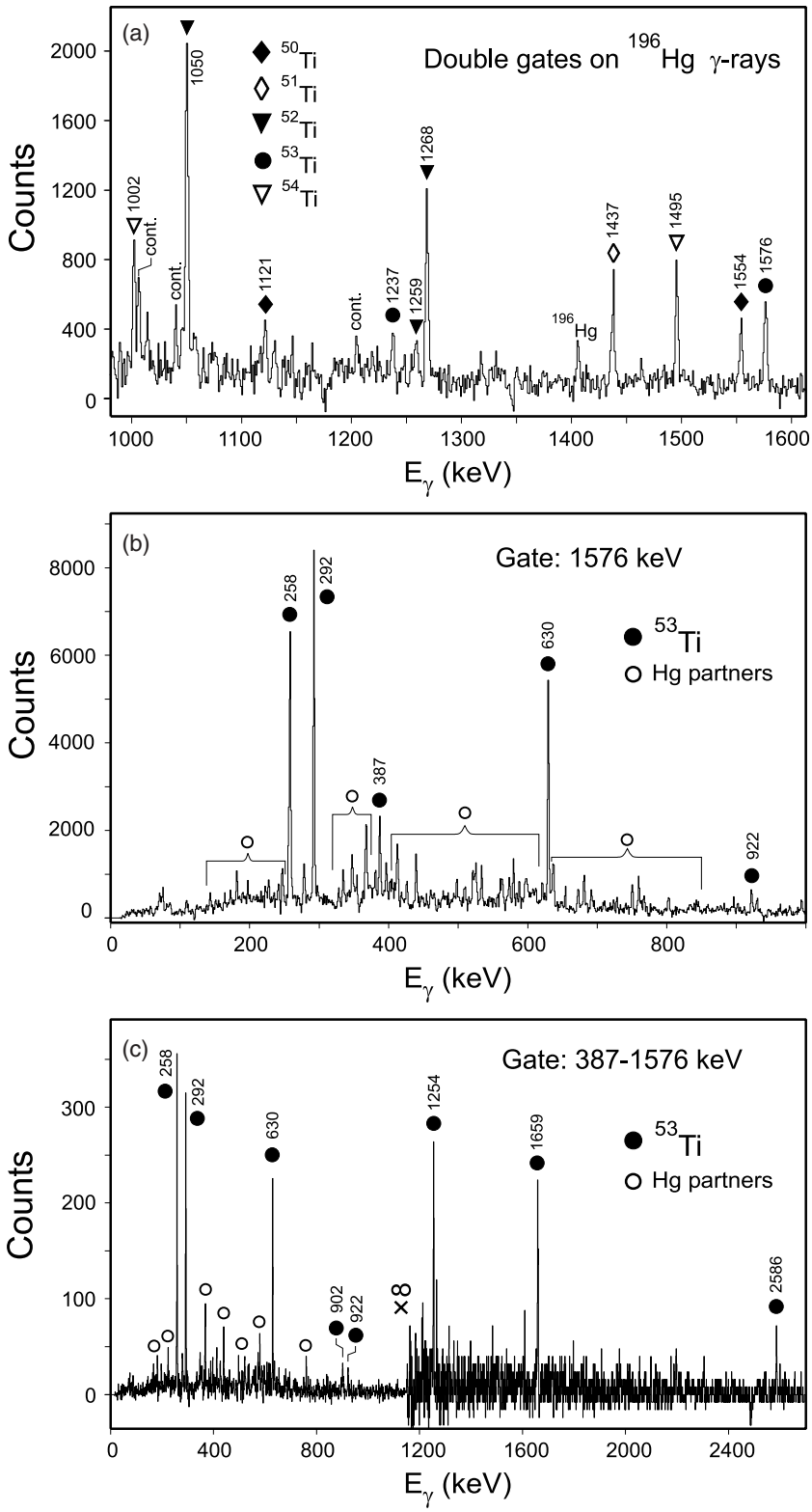

FIG. 1. Representative γ-ray spectra from the ^{48}Ca+^{208}Pb reaction: (a) part of a coincidence spectrum gated on pairs of yrast transitions in ^{196}Hg showing γ rays belonging to Ti partners, (b) spectrum from the $\gamma\gamma$ coincidence matrix gated on the 1576 keV line (assigned to ^{53}Ti), (c) double coincidence gate on selected ^{53}Ti γ rays used to find higher spin transitions in the nucleus. Note that the energy scale in the three panels is different.

from the calculated coefficients [12] is about 1.14, while a $3 \rightarrow 1 \rightarrow 0$ stretched cascade will give 0.91. However, for mixed $M1/E2$ transitions, the ratio can vary considerably and depends on the value of the mixing ratio. This has the potential of introducing some ambiguity into the spin-parity assignments. Nevertheless, the difficulty of assigning spin and parity quantum numbers to states with little or no alignment (such as states below isomers) can be avoided to a large degree. The spin and parity assignments proposed hereafter are based on the fact that the reaction feeds yrast states preferentially, on the results of the angular $\gamma\gamma$ correlation analysis, as well as on the γ-decay pattern and on comparisons with

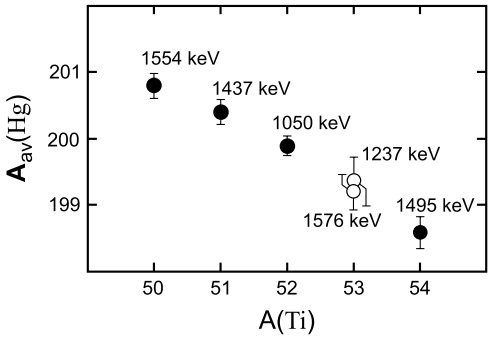

FIG. 2. Plot of average mass A_{av}(Hg) of complementary Hg fragments against Ti product mass A(Ti) deduced from γ-ray cross-coincidence intensities. A_{av}(Hg) values for the 1576 and 1237 keV transitions have been placed at the expected location in the graph for ^{53}Ti in order to illustrate the justification for their assignment to this nucleus. See text for details.

shell-model calculations (see discussions below). Note that the level scheme of Fig. 4 adopts $3/2^-$ quantum numbers for the ^{53}Ti ground state, in agreement with Ref. [13] and with the systematics.

Tables I and II summarize the results of the various measurements by presenting the transition energies and intensities for the two reactions as well as the measured angular correlation coefficients and the proposed assignments. In Table II, it can be noticed that the first four entries concern cascades of the $E2 \rightarrow M1/E2$ type. From the analysis, the $M1/E2$ mixing ratios, expressed as arctan (δ), have been obtained. The derived values are consistent with those extracted for the last four entries in Table II, which relate to $M1/E2 \rightarrow M1/E2$ cascades. For example, the 1576 $\rightarrow$ 630 correlation translates into a mixing of arctan (δ) = 0.76°(2), while the mixing for the 1576 $\rightarrow$ 292 correlation gives arctan (δ) = -3°(1). These two mixing values in turn result in a computed correlation coefficient $I_\gamma(28°)/I_\gamma(85°) = 1.09(2)$ which agrees with the 1.10(2) measured value of Table II for the 630 $\rightarrow$ 292 sequence.

TABLE II. Angular correlation coefficients measured for pairs of transitions in ^{53}Ti following the method described in the text. Adopted spin assignments are given in the last column.

$E_{\gamma 1}$-$E_{\gamma 2}$	$I_\gamma(28°)/I_\gamma(85°)$	$(J_1^\pi \rightarrow J_2^\pi)$-$(J_3^\pi \rightarrow J_4^\pi)$
1576-630	0.91(2)	$(7/2^- \rightarrow 3/2^-)$-$(9/2^- \rightarrow 7/2^-)$
1576-292	0.95(2)	$(7/2^- \rightarrow 3/2^-)$-$(11/2^- \rightarrow 9/2^-)$
1576-258	0.81(2)	$(7/2^- \rightarrow 3/2^-)$-$(13/2^- \rightarrow 11/2^-)$
1576-387	0.68(2)	$(7/2^- \rightarrow 3/2^-)$-$(15/2^- \rightarrow 13/2^-)$
630-292	1.10(2)	$(9/2^- \rightarrow 7/2^-)$-$(11/2^- \rightarrow 9/2^-)$
292-258	1.43(3)	$(11/2^- \rightarrow 9/2^-)$-$(13/2^- \rightarrow 11/2^-)$
292-387	1.54(4)	$(11/2^- \rightarrow 9/2^-)$-$(15/2^- \rightarrow 13/2^-)$
292-1237	1.21(3)	$(11/2^- \rightarrow 9/2^-)$-$(5/2^- \rightarrow 3/2^-)$

III. DISCUSSION

Recently, a new effective interaction for the full *pf* shell, labeled GXPF1, was developed by Honma *et al.* [14], and shell-model calculations with this interaction were found to be quite successful in describing the features associated with the $\nu p_{3/2}$ subshell closure at $N = 32$ in neutron-rich nuclei above ^{48}Ca. Specifically, the GXPF1 Hamiltonian gives a good description of the variations in the $E(2_1^+)$ energies in the Cr, Ti, and Ca isotopic chains near $N = 32$ [14] and accounts reasonably well for the high-spin states in the ^{50,52,54}Ti isotopes [4]. The interaction also reproduces the magnitude of the $B(E2; 0^+ \rightarrow 2_1^+)$ reduced transition rates in

TABLE I. Levels with spin-parity assignments and γ rays identified in ^{53}Ti, including intensities, placements, and branching ratios from the ^{48}Ca+^{238}U reaction. γ-ray branching ratios calculated using the GXPF1 Hamiltonian are shown for comparison.

E_{level} [keV]	J^π	E_γ [keV]	I_γ [rel. units]	Experimental branching ratio	Calculated branching ratio
1237	$5/2^-$	1237.1(2)	45(5)		
1576	$7/2^-$	339.4(3)	33(5)	0.18(2)	0.16
		1576.2(2)	100	0.82(5)	0.84
2206	$9/2^-$	629.6(2)	86(5)	0.91(7)	0.86
		968.6(5)	9(2)	0.09(3)	0.14
2498	$11/2^-$	292.3(2)	77(5)	0.89(8)	0.81
		921.8(4)	13(2)	0.11(3)	0.19
2756	$13/2^-$	257.8(2)	65(5)		
3143	$15/2^-$	387.2(2)	28(2)		
4802	$(17/2^-)$	1659.2(4)	9(2)		
5729	$(17/2^-)$	2586.1(5)	5(1)		
6056	$(21/2^-)$	1254.4(4)	8(2)		
6630		574.4(6)	2(0.5)		
		901.6(4)	5(1)		
		1828(1)	<0.5		
8131		1500.7(6)	3(1)		

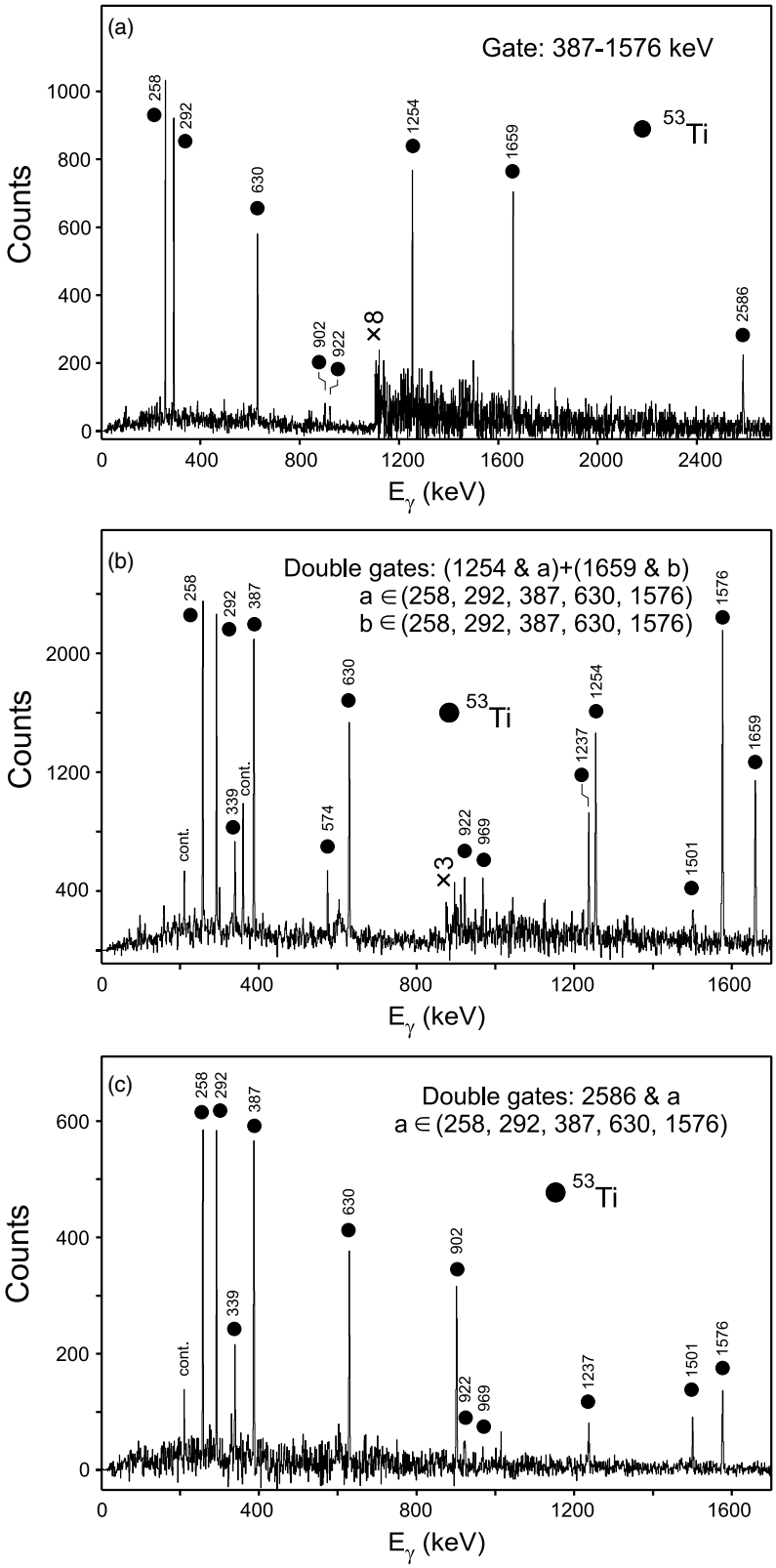

FIG. 3. Representative γ-ray spectra from the ^{48}Ca+^{238}U reaction: (a) double coincidence gate on selected ^{53}Ti γ rays illustrating the quality of data collected with Gammasphere, (b) sum of double gates on selected ^{53}Ti γ transitions used to find higher spin transitions in the nucleus, (c) similar to (b), but for another selection of double gates. Note the difference in the energy scale in panel (a) with respect to (b) and (c).

^{48,50,52,54}Ti, but fails to account for the measured variations of this quantity with mass [15]. The $N = 32$ subshell closure has been attributed to the combined actions of the $\nu 2p_{3/2}$-$\nu 2p_{1/2}$ spin-orbit splitting and the weakening of the $\pi f_{7/2}$-$\nu f_{5/2}$ monopole interaction strength as protons are removed from the $\pi f_{7/2}$ orbital resulting in the migration of the $\nu f_{5/2}$ level to higher energies [3].

Another empirical Hamiltonian constructed for nuclei in the *pf* shell is the FPD6 interaction [16]. Calculations with this Hamiltonian are not as successful as those with the GXPF1

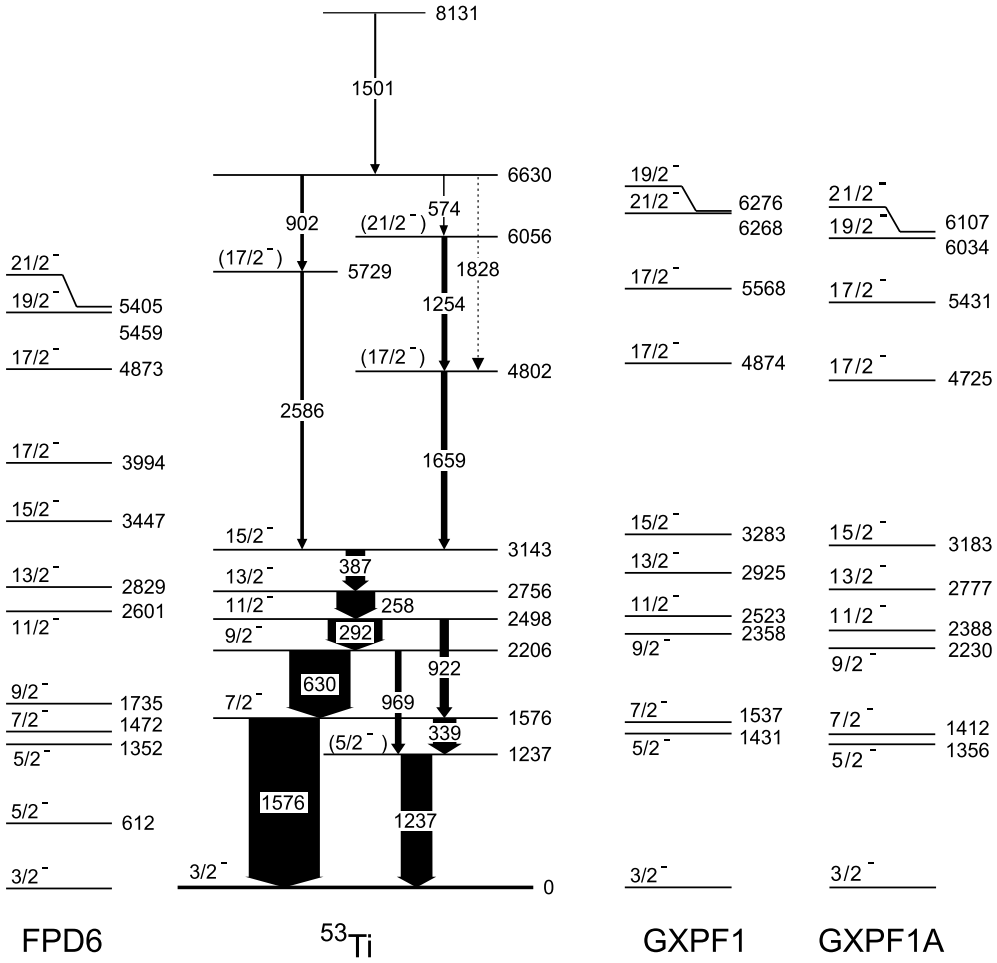

FIG. 4. Proposed level scheme for ^{53}Ti and results of the full-*pf*-shell-model calculations using the GXPF1, FPD6, and GXPF1A interactions.

interaction in reproducing the $E(2_1^+)$ energy systematics in ^{50,52,54}Ti nuclei nor in accounting for the high-spin structures of these even-even Ti nuclei [4,7]. Nevertheless, as shown below, the comparison of the results obtained for ^{53}Ti with both interactions is instructive, and both sets of calculations can be found in Fig. 4. The agreement with experiment is good, especially for the GXPF1 interaction, and the results from this Hamiltonian often provided guidance for the spin-parity assignments proposed in the measured level scheme. Table I compares the experimental branching ratios for the decay of the various ^{53}Ti states with those computed with the GXPF1 interaction: the agreement is again satisfactory and can be regarded as further support for the spin-parity assignments.

The yrast states in ^{53}Ti, calculated with both the GXPF1 and FPD6 Hamiltonians, have a remarkably simple interpretation: in most instances, the associated wave functions are dominated, at the 40–70% level, by a single shell-model component. Thus, the low-lying yrast levels, with spins up to $I = 15/2$, are understood as members of the $\pi f_{7/2}^2 \nu f_{7/2}^8 p_{3/2}^3$ multiplet. The next high-spin levels in the yrast sequence, e.g., the $17/2_1^-$ and $17/2_2^-$ states, are interpreted as corresponding to a mixture of the $\pi f_{7/2}^2 \nu f_{7/2}^8 p_{3/2}^2 p_{1/2}$ and $\pi f_{7/2}^2 \nu f_{7/2}^8 p_{3/2}^2 f_{5/2}$ configurations, while the excitation with the highest spin, the $21/2^-$ state, is dominated by the $\pi f_{7/2}^2 \nu f_{7/2}^8 p_{3/2}^2 f_{5/2}$ configuration.

One of the predictions based on the GXPF1 interaction is the onset of significant energy gaps between the effective neutron single-particle energies associated with the $\nu p_{3/2}$, $\nu p_{1/2}$, and $\nu f_{5/2}$ orbitals in neutron-rich nuclei with the latter two states lying 1.7 and 4.0 MeV above the former in ^{53}Ti. In contrast, the calculations with the FPD6 Hamiltonian do not exhibit the same gaps. In this case, the $\nu f_{5/2}$ state is 2.1 MeV above the $\nu p_{3/2}$ orbital and lies lower than the $\nu p_{1/2}$ level from which it is separated by only 880 keV. Since the neutron orbitals of interest are involved in the configurations of the ^{53}Ti high-spin yrast states, a more detailed comparison between the experimental energies and the results of the shell-model predictions with both interactions is warranted. The $17/2_1^-$, $17/2_2^-$, and $21/2^-$ states are of particular interest since their wave functions involve a neutron in either the $p_{1/2}$ or $f_{5/2}$ orbital and their excitation energies depend on the relative effective single-particle energies of the $\nu p_{3/2}$, $\nu p_{1/2}$, and $\nu f_{5/2}$ states. As seen in Fig. 4, the GXPF1 calculations give a much better description of the experimental level sequence than those with FPD6. For example, the GXPF1 Hamiltonian only slightly overestimates the energies of the three states

by an average of 120 keV, whereas the FPD6 calculations underestimate the energy of the same levels by an average of 770 keV. Also, the energy spacings between the members of the $\pi f_{7/2}^2 \nu f_{7/2}^8 p_{3/2}^3$ multiplet are accounted for in a better way with the GXPF1 Hamiltonian.

Differences in the predictions of the two Hamiltonians regarding the energy of the $17/2_1^-$, $17/2_2^-$, and $21/2^-$ states can be associated with differences in the effective single-particle energies of the $\nu p_{1/2}$ and $\nu f_{5/2}$ orbitals with respect to the $\nu p_{3/2}$ state. As stated above, in the FPD6 calculations around ^{53}Ti, the effective single-particle energy of the $\nu f_{5/2}$ state is close to that of $\nu p_{1/2}$ orbital, and the energy spacings between both these states and the $\nu p_{3/2}$ orbital are rather small as well. In contrast, in the GXPF1 Hamiltonian, the $\nu f_{5/2}$ level is located quite high above the $\nu p_{1/2}$ single-particle state, and there is also sizable splitting between the $\nu p_{3/2}$ and $\nu p_{1/2}$ orbitals. The present results for ^{53}Ti then suggest that the actual separation between the $\nu p_{3/2}$ state and the $\nu p_{1/2}$ and $\nu f_{5/2}$ pair is close to that predicted by the GXPF1 Hamiltonian, and that this gap is too small in the FPD6 case.

Whether a sizable energy gap exists between the effective single-particle energies associated with the $\nu p_{1/2}$ and $\nu f_{5/2}$ orbitals in neutron-rich nuclei, as predicted by the GXPF1 interaction, cannot be unambiguously answered through the above comparisons with the ^{53}Ti data. This issue is important, however, as a substantial $\nu p_{1/2}$-$\nu f_{5/2}$ gap leads to a subshell closure at $N = 34$ that should be apparent in the energy spacings observed for the low-lying levels of ^{54}Ca and ^{56}Ti, for example. The excitation energies of the $17/2_1^-$ and $21/2^-$ yrast states in ^{53}Ti provide the sole means of testing this aspect of the interaction with the present data. These two levels are calculated to lie at an energy higher than the experimental value by $\sim$70 and $\sim$210 keV, respectively. This comparison is in line with earlier observations for ^{54}Ti, where GXPF1 calculations reproduce the low-spin yrast sequence very well but overpredict the energies of higher spin states whose wave functions are dominated by configurations including a $f_{5/2}$ neutron. These findings can be taken together with recent results on ^{56}Ti from Refs. [5–7] to argue for a smaller gap between the $\nu p_{1/2}$ and $\nu f_{5/2}$ orbitals than the GXPF1 interaction calculates. Indeed, in ^{56}Ti, the calculated energies $E(2_1^+) = 1516$, $E(4_1^+) = 2529$, and $E(6_1^+) = 3044$ keV differ significantly from the experimental sequence of 1129, 2290, and 2980 keV.

With all these observations in mind, the GXPF1 Hamiltonian was modified recently in order to reproduce the low-lying levels in ^{56}Ti. Five $T = 1$ matrix elements involving mainly the $\nu p_{1/2}$ and $\nu f_{5/2}$ single-particle orbitals were changed [17]. Specifically, more repulsive monopole pairing strengths were adopted for the $p_{1/2}$-$p_{1/2}$ and $p_{1/2}$-$f_{5/2}$ couplings, while the quadrupole-quadrupole interaction between $p_{1/2}$-$f_{5/2}$ orbitals was made more attractive. In addition, a slightly more repulsive $f_{7/2}$-$f_{7/2}$ monopole pairing was adopted as well. The resulting $\nu p_{1/2}$-$\nu f_{5/2}$ gap in the effective single-particle energies becomes narrower by $\sim$0.5 MeV for $N \geqslant 34$, and the mixing among the two states becomes larger than in the case with the GXPF1 interaction. The modified interaction has been designated as GXPF1A and, naturally, provides a satisfactory description of the low-lying excitations in ^{56}Ti [15,17].

The results of the full-*pf*-shell-model calculations with the GXPF1A Hamiltonian for ^{53}Ti can also be found in Fig. 4. As discussed above, the excitations involving the $\nu p_{1/2}$ and $\nu f_{5/2}$ orbitals, i.e., the $17/2_1^-$, $17/2_2^-$, and $21/2^-$ states, are expected to be particularly sensitive to the modifications of the GXPF1 interaction. The $17/2_1^-$ and $21/2^-$ states are calculated to lie at 4725 and 6107 keV, respectively, in close agreement with the measured energies of 4802 and 6056 keV. The comparison is somewhat worse for the $17/2_2^-$ excitation, located at 5729 keV and computed at 5431 keV, but this most likely reflects deficiencies in the description of the configuration mixing.

The satisfactory agreement of the shell-model calculations with the modified GXPF1 interaction, GXPF1A, for both ^{53}Ti and ^{56}Ti bolsters confidence in predictions for other nuclei. As stated in Ref. [15], it is noteworthy that the energy separation between the $\nu p_{1/2}$ and $\nu f_{5/2}$ orbitals obtained with the GXPF1A Hamiltonian increases with the removal of the last two protons from the $\pi f_{7/2}$ orbital. As a result, a subshell closure may still occur at $N = 34$ in the Ca nuclei, and further investigations of the structure of neutron-rich Ca isotopes are required to settle the issue.

IV. CONCLUSIONS

γ-ray coincidence measurements using Gammasphere with the ^{48}Ca+^{208}Pb and the ^{48}Ca+^{238}U reactions have provided information on the yrast excitations in the neutron-rich ^{53}Ti isotope. Transitions between the lowest levels in ^{53}Ti were identified using the γ-ray cross-coincidence technique between reaction partners. Subsequently, these transitions were used to locate states with spins up to $I^\pi = 21/2^-$. The yrast structure of ^{53}Ti was compared with the results of shell-model calculations performed with the GXPF1 and FPD6 interactions. The experimental data are particularly well described by the GXPF1 calculations. This observation is directly related to the fact that the $\nu f_{5/2}$ and $\nu p_{1/2}$ orbitals are well separated from the $\nu p_{3/2}$ state, a fact that also gives rise to the subshell closure at $N = 32$.

The ^{53}Ti level scheme is reproduced equally well, if not better, by shell-model calculations using a modified version of the GXPF1 interaction, labeled GXPF1A, adjusted to take into account recent experimental results on the ^{56}Ti low-spin yrast sequence. According to the predictions based on this new GXPF1A interaction, the $\nu f_{5/2}$ orbital is not separated from the $\nu p_{1/2}$ state to the extent implied by the GXPF1 Hamiltonian, and this prevents subshell closure at $N = 34$ in the Ti isotopes. The calculations with the GXPF1A Hamiltonian provide a very consistent description of the known yrast structures along the entire chain of neutron-rich Ti isotopes. In addition, a significant energy gap at $N = 34$ is still predicted to occur in the Ca isotopes.

ACKNOWLEDGMENTS

The authors thank the ATLAS operating staff for the efficient running of the accelerator and John Greene for

preparing the targets used in the measurement. This work was supported by the U.S. Department of Energy, Office of Nuclear Physics, under Contracts No. W31-109-ENG-38 by National Science Foundation Grant Nos. PHY-01-01253, PHY-00-70911, and PHY-97-24299, and by Polish Scientific Committee Grant No. 2PO3B-074-18.

[1] T. Otsuka, R. Fujimoto, Y. Utsuno, B. A. Brown, M. Honma, and T. Mizusaki, Phys. Rev. Lett. **87**, 082502 (2001).
[2] A. Huck, G. Klotz, A. Knipper, C. Miehe, C. Richard-Serre, G. Walter, A. Poves, H. L. Ravn, and G. Marguier, Phys. Rev. C **31**, 2226 (1985).
[3] J. I. Prisciandaro, P. F. Mantica, B. A. Brown, D. W. Anthony, M. W. Cooper, A. Garcia, D. E. Groh, A. Komives, W. Kumarasiri, P. A. Lofy *et al*., Phys. Lett. **B510**, 17 (2001).
[4] R. V. F. Janssens *et al*., Phys. Lett. **B546**, 55 (2002).
[5] S. N. Liddick *et al*., Phys. Rev. Lett. **92**, 072502 (2004).
[6] S. N. Liddick *et al*., Phys. Rev. C **70**, 064303 (2004).
[7] B. Fornal *et al*., Phys. Rev. C **70**, 064304 (2004).
[8] B. Fornal *et al*., Acta. Phys. Pol. B **26**, 357 (1995).
[9] R. Broda, Eur. Phys. J. A **13**, 1 (2002) and references therein.
[10] W. Krolas *et al*., Nucl. Phys. **A724**, 289 (2003).
[11] I. Y. Lee, Nucl. Phys. **A520**, 641c (1990).
[12] K. S. Krane, R. M. Steffen, and R. M. Wheeler, Nuclear Data Tables **11**, 351 (1973); R. M. Steffen, and K. Alder, in *The Electromagnetic Interaction in Nuclear Physics*, edited by W. D. Hamilton (North-Holland, Amsterdam, 1973).
[13] L. A. Parks, C. N. Davids, and R. C. Pardo, Phys. Rev. C **15**, 730 (1977); H. Junde, Nucl. Data Sheets **87**, 507 (1999).
[14] M. Honma, T. Otsuka, B. A. Brown, and T. Mizusaki, Phys. Rev. C **65**, 061301(R) (2002).
[15] D. C. Dinca *et al*., Phys. Rev. C **71**, 041302(R) (2005).
[16] W. A. Richter, M. G. Van Der Merwe, R. E. Julies, and B. A. Brown, Nucl. Phys. **A523**, 325 (1991).
[17] M. Honma *et al*., in Proceedings of the ENAM'04 Conference, Callaway Gardens, Pine Mountain, Georgia, September 12–16, 2004, Eur. Phys. J. A **25**, 499 (2005).